Cooperative Interaction of Arginine-19 and the N-Terminal Signaling Domain in the Affinity and Potency of Parathyroid Hormone†

Natia Tsomaia,‡ Masaru Shimizu,§ Naoto Shimizu,§ Thomas J. Gardella,§ and Dale F. Mierke*,‡,||

Department of Molecular Pharmacology, Division of Biology and Medicine, and Department of Chemistry, Brown University, Providence, Rhode Island 02912, and Endocrine Unit, Massachusetts General Hospital and Harvard Medical School, Boston, Massachusetts 02114

Received November 26, 2003; Revised Manuscript Received January 28, 2004

ABSTRACT: Residue 19 of parathyroid hormone (PTH) plays a unique role in the interaction process with the PTH1 receptor. A $Glu^{19} \rightarrow Arg^{19}$ substitution, based on the Arg^{19} of the PTH-related protein (PTHrP), increases the binding affinity when incorporated into the N-terminus of PTH [i.e., PTH(1−20)] and has no effect when introduced into the C-terminus of PTH [i.e., PTH(15−31)]. To explore Arg^{19} and the midregion (residues 10−15), we designed the novel PTH scaffold peptide, PG5, which has the PTH(1−9) domain linked to the PTH(15−31) segment via a pentaglycine spacer. Substitution of Glu^{19} with Arg^{19} in PG5 resulted in a 9-fold increase in binding affinity. Additionally, the substitution enhanced stimulated cAMP formation in cells expressing PTH1-delNt, a PTH1 receptor construct lacking most of the N-terminus, confirming that residue 19 is interacting with the juxtamembrane portion of PTH1. The binding and signaling capacities of the PG5 analogues were diminished relative to those of PTH(1−34), indicating that the residue 10−14 region of PTH provides more than just a simple linker function. To probe this further, the structural consequences of the glycine linker and its interaction with PTH1 were examined by circular dichroism, ^{1}H NMR, and extensive ligand/receptor molecular dynamics simulations. The structural data clearly illustrate the helix-stabilizing effect of Arg^{19} substitution propagating N-terminally from position 19 to the pentaglycine linker. Overall, these studies suggest that an α-helix is the preferred conformation for the residue 15−20 region of PTH and that residues 10−14 are also required for full affinity and potency of the hormone.

Parathyroid hormone (PTH)[1] is the major regulator of the ionized calcium level in the human body. The 84 amino acid peptide adjusts the calcium fluctuations in the blood caused by bone remodeling, renal function, and dietary intake. PTH functions through the activation of the cell surface receptor type 1 (PTH1). This receptor belongs to the class 2 family of the seven transmembrane G protein-coupled receptors (GPCRs) and is mainly expressed in kidney and bone. All functions of PTH are encoded within the first 34 amino acids of the hormone (*1*−*6*); PTH(1−34) is capable of high-affinity binding and activation of the PTH1 receptor. The PTH1 also mediates the actions of the PTH-related peptide (PTHrP), a key developmental protein that is also secreted by many tumors resulting in the hypercalcemia of malignancy. As for PTH, the PTHrP(1−34) peptide is fully potent on the PTH1, and the two ligands share N-terminal homology with 8 identities in the first 13 residue positions. The shortened analogue PTH(1−31) displays adenylyl cyclase stimulating activity comparable to that of PTH(1−34), and both PTH-(1−31) and PTH(1−34) mediate potent anabolic responses in bone (*7*). Due to their anabolic effects on bone density, PTH analogues may represent a new family of therapeutics for the treatment of osteoporosis (*8*).

To understand the bioactive conformation of PTH and its mechanism of interaction with PTH1, a large number of truncated and modified PTH analogues have been studied. High-resolution solution NMR studies have repeatedly shown the presence of a short α-helix, typically including the N-terminal residues 3−11, and a well-defined α-helical region, usually spanning through residues 17−30 (*9*, *10*). Experimental evidence demonstrates that the major determinants for receptor activation are located in the N-terminal domain (residues 1−9) of PTH(1−34) (*6*), while the C-terminus (approximately residues 15−34) is responsible for PTH1 binding affinity (*2*, *3*). According to the current two-domain hypothesis, the C-terminal portion of PTH(1−34) interacts with the amino-terminal extracellular ("N") domain

† Supported, in part, by the National Institutes of Health though Grants DK-11794 (T.J.G.) and GM-82054 (D.F.M.).

* Address correspondence to this author at the Department of Molecular Pharmacology, 171 Meeting St., Brown University, Providence, RI 02912. Voice: (401) 863-2139. Fax: (401) 963-1595. E-mail: Dale_Mierke@Brown.edu.

‡ Department of Molecular Pharmacology, Division of Biology and Medicine, Brown University.

§ Endocrine Unit, Massachusetts General Hospital and Harvard Medical School.

|| Department of Chemistry, Brown University.

[1] Abbreviations: PTH, parathyroid hormone; r, rat; h, human; PTHrP, PTH-related protein; PTH1, type 1 PTH/PTHrP receptor; DPC, dodecylphosphocholine; NMR, nuclear magnetic resonance; DG, distance geometry; MD, molecular dynamics; NOE, nuclear Overhauser effect; NOESY, nuclear Overhauser effect spectroscopy; TOCSY, total correlation spectroscopy; RMSD, root-mean-square deviation; CD, circular dichroism; TM, transmembrane; EC, extracellular loop; ECM, extracellular matrix; IBMX, 3-isobutyl-1-methylxanthine; Bpa, benzoylphenylalanine; Nle, norleucine. Other amino acids are in the conventional one- or three-letter codes.

10.1021/bi036127t CCC: $27.50
Published on Web 03/04/2004

Table 1: Peptide Primary Structures

peptide name	sequence[a]
PTH(1−34)	S-V-S-E-I-Q-L-M-H-N-L-G-K-H-L-N-S-M-**E**-R-V-E-W-L-R-K-K-L-Q-D-V-H-N-Y-amide
PTH(1−9)Gly5PTH(15−31) or PG5	A-V-S-E-I-Q-L-M-H-G-G-G-G-G-L-N-S-M-**E**-R-V-E-W-L-R-K-K-L-Q-D-V-amide
PTH(1−9)Gly5[Arg^{19}]PTH(15−31) or [Arg^{19}]PG5	A-V-S-E-I-Q-L-M-H-G-G-G-G-G-L-N-S-M-**R**-R-V-E-W-L-R-K-K-L-Q-D-V-amide
PTH(15−31)	L-N-S-M-**E**-R-V-E-W-L-R-K-K-L-Q-D-V-amide
[Arg^{19}]PTH(15−31)	L-N-S-M-**R**-R-V-E-W-L-R-K-K-L-Q-D-V-amide
tracer analogue bPTH(3−34)	S-E-I-Q-F-Nle-H-N-L-G-K-H-L-S-S-Nle-E-R-V-E-W-L-R-K-K-L-Q-D-V-H-N-Y*-amide

[a] Peptide sequences are shown N-terminal to C-terminal with amino acids represented by the conventional one-letter code, with the exception of norleucine (Nle). Peptides are derivatives of human PTH, with the exception of b (bovine) PTH(3−34). Each peptide contained a free amino terminus and a carboxamide at the C-terminus. The asterisk on the Tyr of the tracer radioligand analogues indicates the position of the ^{125}I atom.

of the PTH1 providing the majority of the binding energy, and the N-terminus of the ligand interacts with the juxtamembrane ("J") region of the PTH1 to induce receptor activation (*11*). A bihelical structure for the ligand may predominate in the receptor interaction process, as suggested by the above NMR-based structural investigations. However, the finding that a PTH(1−31) analogue containing three lactam bridges (Lys^{13}−Asp^{17}, Lys^{18}−Asp^{22}, Lys^{26}−Asp^{30}) enhancing helical structure behaves as a highly potent agonist suggests that at least one bioactive form of the ligand contains an α-helix spanning at least residues 13−30 (*12*). Additionally, the X-ray crystal structure of PTH(1−34), in fact, reveals a single α-helix extending from residue 2 to residue 32 (*13*). Altogether, there is still a great deal of ambiguity in our current view of the bioactive conformation of PTH and the mechanism by which it interacts with the receptor.

Much effort has been devoted to the identification and characterization of structural components in the ligand that mediate the PTH/PTH1 interaction process. Residue 19 (Glu in PTH and Arg in PTHrP) has been shown to be a key determinant of bioactivity. We have recently shown that this residue plays an important role in both binding to and activation of PTH1; specifically, the substitution of Glu^{19} → Arg in both PTH(1−34) and PTH(1−20) analogues enhances the capacities of the ligands to interact with the PTH1 J domain, as represented by the mutant PTH1 construct, PTH1-delNt, which lacks most of the N domain (*14*). We have previously shown (*15*) by CD and NMR spectroscopy data that the Glu^{19} → Arg substitution in the PTH(1−34) and PTH(1−20) peptides increases helical content. The combined data, therefore, suggested that residue 19 must be α-helical for optimal interaction with the J domain of the receptor. In addition, our in vitro data showed that the Arg^{19} effect requires the presence of residues 1−14 of PTH, as the Glu^{19} → Arg substitution does not alter the binding affinity of PTH(15−31). This finding suggested that Arg^{19} positively contributes to the capacity of the N-terminal (1−14) region of the ligand to interact with the juxtamembrane region of PTH1; however, the mechanism underlying this effect remained to be determined.

To explore the pathways by which residue 19 influences ligand action and its apparent effect on the N-terminal signaling domain of PTH, we designed and synthesized two new PTH(1−31) analogues in which the N- and C-terminal domains are connected by a flexible, pentaglycine spacer. We pharmacologically characterized the resulting analogues, PTH(1−9)Gly5PTH(15−31) (PG5) and PTH(1−9)Gly5-[Arg^{19}]PTH(15−31) ([Arg^{19}]PG5), in PTH1-transfected cell systems; furthermore, we described in detail the structural changes that may be responsible for the observed biological activities using circular dichroism and solution-state NMR spectroscopic techniques. Finally, we performed extensive molecular dynamics simulations, carried out in a three-phase (water/decane/water) membrane-mimicking environment, to assess the docking of these ligands to the full-length PTH1 receptor. The overall results provide new insight into the mechanism by which residue 19, as well as the residue 10−15 region, of parathyroid hormone contributes to biological activity.

EXPERIMENTAL PROCEDURES

Peptides. All peptides utilized in this study (Table 1) contained a free amino terminus and a carboxamide at the C-terminus. The control peptide used was [Tyr^{34}]hPTH(1−34)NH_2 [PTH(1−34)]. The peptide [Nle^{8,18},Tyr^{34}]bPTH(3−34)NH_2 [PTH(3−34)] was purchased from Bachem (Torrance, CA). All other peptides were prepared on an Applied Biosystems model 430A peptide synthesizer using Fmoc main-chain protecting group chemistry, HBTU/HOBt/DIEA (1:1:2 molar ratio) for coupling reactions, and TFA-mediated cleavage/side chain deprotection (MGH Biopolymer Synthesis Facility, Boston, MA). Crude peptides were desalted by adsorption on a C18-containing cartridge and purified further by HPLC. Peptides were dissolved in 10 mM acetic acid and stored at −80 °C. The purity, identity, and stock concentration of each peptide were secured by analytical HPLC, matrix-assisted laser desorption/ionization (MALDI) mass spectrometry, and amino acid analysis. Radiolabeling of PTH(3−34) was performed using ^{125}INa (2200 Ci/mmol; NEN) and chloramine-T; the resultant ^{125}I-PTH(3−34) was purified by HPLC.

Cell Culture. Cells were cultured at 37 °C in T-75 flasks (75 mM) in Dulbecco's modified Eagle's medium (DMEM) supplemented with fetal bovine serum (10%), penicillin G (20 units/mL), streptomycin sulfate (20 μg/mL), and amphotericin B (0.05 μg/mL) in a humidified atmosphere containing 5% CO_2 (Hyclone Laboratories, Logan, UT); stock solutions of trypsin/EGTA and antibiotics were from GIBCO. Cells were subcultured in 24-well plates prior to transfection and assay. COS-7 cells were transiently transfected with pCDNA1-based plasmids encoding either the intact wild-type human PTH-1 receptor (PTH1) or the N-terminally truncated human PTH1 construct, PTH1-delNt, using DEAE-dextran and 200 ng of cesium chloride-purified plasmid DNA per well, as described previously (*16*). Four days after transfection the cells were used for assay. The HKRK-B28 cell line was derived from the porcine kidney cell line LLC-PK_1 by stable transfection with the pCDNA1-

based plasmid encoding the intact PTH1 and expresses 280000 PTH receptors per cell (*17*). HKRK-B28 cells were used for assay 24−48 h after confluency was attained.

cAMP Stimulation and Competition Binding Assays. Stimulation of cells with peptide analogues was performed in 24-well plates. Binding reactions containing ca. 100000 cpm of ^{125}I-PTH(3−34) (ca. 26 fmol; final volume = 300 μL) were incubated 4 h at 15 °C. Cells were then placed on ice, the binding medium was removed, and the monolayer was rinsed three times with 0.5 mL of cold binding buffer. The cells were subsequently lysed with 0.5 mL of 5 N NaOH and counted for radioactivity. The nonspecific binding was determined by competition with a 1 μM dose of unlabeled [Nle^{8,21},Tyr^{34}]rPTH(1−34)NH$_2$.

Data Calculation. Calculations were performed using Microsoft Excel. The cAMP EC_{50} values and the corresponding maximum response (E_{max}) values and IC_{50} values were calculated using nonlinear regression using the four-parameter equation $y_p = \min + [(\max - \min)/(1 + (IC_{50}/x)^{slope})]$ and the Excel Solver function for parameter optimization (*18*). The statistical significance between two data sets was determined using a one-tailed Student's *t*-test, assuming unequal variances for the two sets.

Circular Dichroism. Circular dichroism spectra were recorded on a Jasco model 710 spectropolarimeter; peptides were analyzed at a concentration of 50 μM in 50 mM sodium phosphate buffer, pH 7.4, containing 2,2,2-trifluoroethanol (TFE) at 20% (v/v). Spectroscopic scans were performed at 20 °C and at wavelengths between 185 and 255 nm, with data recorded at each 1 nm interval. Eight scans were accumulated and averaged for each sample. At each wavelength, the mean residue molar elipticity [θ] (in dimensions of deg·cm/dmol) was calculated by the equation $[\theta] = \theta \times 100/lCn$, where θ is the raw ellipticity value (in dimensions of millidegree), l is the sample path length in centimeters, C is the molar peptide concentration, and n is the number of residues in the peptide (*19*). The helical content of each peptide was estimated by dividing [θ] observed at 222 nm for that peptide by −33100 (*19*, *20*).

NMR Experiments. Solution samples were made by dissolving 3.1 mg of solid peptide in 600 μL of a 50 mM phosphate buffer (pH = 6.5, uncorrected for isotope effect), which contained 5% D_2O and 180 mM dodecylphosphocholine-d_{38} (DPC; Cambridge Isotopes Laboratories).

The NMR experiments were performed on a Bruker Avance spectrometer operating at a magnetic field strength of 14.09 T (proton resonance frequency of 600.1 MHz). The reported chemical shift values for ^{1}H are expressed in parts per million and internally referenced to proton resonance from sodium 3-(trimethylsilyl)tetradeuteriopropionate (TSP) at 0.0 ppm.

Data were collected at 298 and 308 K. In both peptides, the amino acid sequence was identified using TOCSY experiments (*21*), which employed the MLEV-17 pulse sequence for Hartmann−Hahn transfer (*22*). Mixing times ranged between 30 and 65 ms with a spin-lock field strength of 10 kHz. The sequential assignment and proton−proton distances were obtained from NOESY experiments employing mixing times of 100 and 200 ms (*23*, *24*). The WATERGATE sequence was used to achieve water suppression (*25*).

All two-dimensional spectra were acquired using the time-proportional phase incrementation method (*26*), collecting 640 FIDs of 2048 data points. Spectra were processed using the NMRPipe software (*27*). The time domain data in both dimensions were multiplied by Gaussian or shifted squared sine-bell window functions, zero-filled to 2048 × 1024 real points, and Fourier transformed. The processed NMR spectra were imported in Sparky software (*28*), where peaks were assigned and integrated. The secondary shift values were calculated relative to reported Hα chemical shifts in random coil conformations and were averaged over three consecutive residues (*29*).

Distance Geometry. Integrated cross-peak volumes from NOESY spectra were converted into distances using the isolated two-spin approximation. During this conversion cross-peak volumes of the resolved methylene β and/or γ protons of Ser^3, Ile^5, Met^8, Met^{18}, Arg^{20}, and Arg^{25} (1.78 Å) and aromatic vicinal protons of Trp^{23} (2.48 Å) were used for calibration. A matrix of experimental upper and lower bounds was created by adding and subtracting 10% to the experimental distance restraints. A pseudoatom correction was applied to the upper bounds of all unresolved methyl and methylene protons (*30*). To obtain the final bound matrix, the experimental restraint matrix was merged with another matrix representing the geometric distance bounds (holonomic constraints). As a result, only NOEs that produce distance restraints tighter than those generated from the molecular constitution were utilized in structure calculations. Using the random metrization algorithm (*31*), typically 100 structures were generated in a four-dimensional space. These structures were optimized by minimizing the distance error function initially in four and then in three dimensions using the conjugate gradient minimization algorithm followed by distance-driven dynamics (*32*, *33*). Structures with NOE violations greater that 0.3 Å were discarded, leaving more than 80 structures fulfilling the experimental proton−proton distances and the canonical (holonomic) constraints for each studied peptide. Dihedral angle order parameters were calculated following Havel (*34*). All calculations were performed on SGI and Pentium III (Linux-based) processors using home-written programs.

MD Simulations. One of the low-penalty function structures, obtained from the metric matrix DG calculations, was chosen for each peptide as a starting structure for the MD simulations. To remove initial strain, each structure was energy minimized in vacuo using conjugate gradients and the AMBER force field, ignoring charges. Minimization was preformed in the DISCOVER (Molecular Simulations, Inc.) program within the molecular modeling package Insight II. Molecular dynamics simulations were performed with the GROMACS program (*35*). To model the water−micelle environment, initially a two-phase simulation box ($x = y = z = 60$ Å), containing typically 5339 water and 305 decane molecules, was constructed. The peptide was then placed at the water/decane interface. Ionizable functional groups at pH = 6.5 were treated as charged species without adding any counterions. All atoms were treated in the GROMOS-87 force field including Lennard-Jones (1.2 nm cutoff), Coulomb (1.2 nm cutoff), and standard bonded (bond stretching, angle bending, improper, and proper dihedrals) interactions. The complete system was energy minimized using the steepest descent algorithm. To optimize solvent−peptide interactions,

a 10 ps long MD simulation with 2 fs time step was performed while the peptide conformation was constrained (force constant was 1000 KJ mol^{-1} nm^{-2}). The experimental constraints were then introduced (force constant was 2000 KJ mol^{-1} nm^{-2}), and the final MD simulations at 300 K (with 0.02 ps temperature bath coupling) were performed for 900 ps. During the simulation an integration time step was 1 fs, and the applied constant pressure was 1 bar. All simulations were performed on Pentium III processors using GROMACS.

Molecular Modeling. The receptor−ligand modeling utilized the NMR-derived structures of PTH(1−9)Gly5PTH-(15−31) and PTH(1−9)Gly5[Arg^{19}]PTH(15−31) analogues. Two molecular models of receptor−ligand complexes, PTH-(1−9)Gly5PTH(15−31)/PTH1 and PTH(1−9)Gly5[Arg^{19}]-PTH(15−31)/PTH1, were constructed on the basis of PTH1 models reported by Rölz et al. (*36*). The PTH analogues examined here were docked to the PTH1, so that the starting structures satisfied previously published contact points from photoaffinity cross-linking studies between the ligand and the receptor. Namely, Val^2/M425 (*37*) Lys^{13}/R186 (*38*) ligand/receptor pairs were placed within 12 Å (between their α carbons). The N-terminal parts of PTH(1−9)Gly5PTH-(15−31)/PTH1 and PTH(1−9)Gly5[Arg^{19}]PTH(15−31)/PTH1 analogues were placed at the extracellular surface of PTH1, above the central core of the 7 TM helical bundle. Backbone dihedral angles of the pentaglycine linkers (flexible region) were rotated manually until the C-terminal helix was in close proximity to the putative PTH1(168−176) helical domain of the N-terminus of the receptor. The resulting receptor−ligand complexes were soaked in a three-layer (water/decane/water) simulation cell to mimic the membrane environment. The TM helices were positioned in a 45 Å thick decane layer, while extra- and intracellular regions were placed in approximately 40 Å thick layers of water above and below. Even though this solvent system does not take into account the charged nature of the lipid/water environment, it provides the essential hydrophilic/hydrophobic interface for MD simulations. Initially, the system in the three-layer box was energy minimized (1000 steps, 300 K). Then, a short MD (10 ps, 300 K) was performed with position restraints applied to the heavy atoms of the receptor and ligand. Finally, distance restraints were introduced with (target value of 12 Å between Val^2/M425 and Lys^{13}/R186 pairs) the force constant 5000 kJ mol^{-1} nm^{-2}, and 100 ps long MD runs (1 fs time step) were performed at 300 K. Then, restraints between the receptor and the ligand were removed, and the system was allowed to evolve freely for the next 500 ps. α-Helices (seven TM helices) within PTH1 were maintained by dihedral angle restraints; the experimental distance restraints (NMR-derived helical NOEs) for the ligands were introduced during MD simulations with the force constant 5000 kJ mol^{-1} nm^{-2}.

RESULTS

Biological Activity. Previously, we showed that the Glu^{19} → Arg modification improved the binding affinity of PTH-(1−20) and PTH(1−34) analogues to PTH1 in HKRK-B28 cells but did not affect the affinity of PTH(15−31) (*14*). To test for possible cooperativity between Arg^{19} and the N-terminus of the ligand, we synthesized PTH(1−9)Gly5PTH-(15−31)NH_2 (PG5) and PTH(1−9)Gly5[Arg^{19}]PTH(15−31)NH_2 ([Arg^{19}]PG5) (Table 1) and functionally compared these analogues in HKRK-B28 cells (Figure 1, Table 2). In competition assays performed with ^{125}I-bPTH(3−34), the apparent affinity observed for [Arg^{19}]PG5 was 9-fold greater than that observed for PG5 (IC_{50}s = 11 ± 1 and 100 ± 30 μM, $P = 0.03$), while in cAMP stimulation assays [Arg^{19}]-PG5 was 13-fold more potent than PG5 (EC_{50}s = 180 ± 40 and 2300 ± 400 nM, $P = 0.006$).

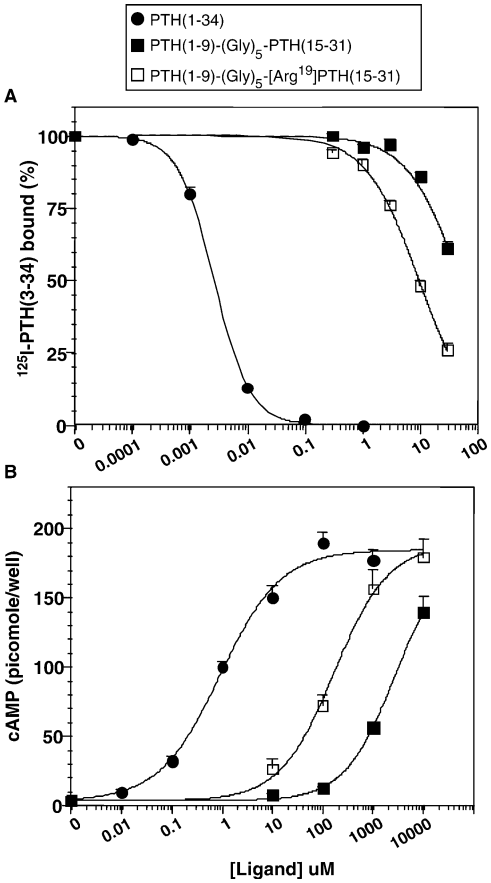

FIGURE 1: Binding and cAMP properties of Gly-linked PTH analogues in HKRK-B28 cells. Two PTH analogues having the (1−9) signaling domain linked via a pentaglycine segment to the PTH(15−31) binding domain containing either Glu (native PTH residue) or Arg at position 19 and the PTH(1−34) control were evaluated in HKRK-B28 cells for the capacity to inhibit the binding of the ^{125}I-[$Nle^{8,18}$,Tyr^{34}]bPTH(3−34)NH_2 tracer radioligand (panel A) or to stimulate cAMP formation (panel B). Data (mean ± sem) shown in (A) were combined from five (5Gly-linked analogues) or four [PTH(1−34) peptide] separate experiments, each performed in duplicate, and those shown in (B) were combined from four (5Gly-linked analogues) or three [PTH(1−34) peptide] separate experiments, each performed in duplicate.

In pilot studies, we synthesized such peptides having various lengths of N-terminal PTH sequences [PTH(1−5), PTH(1−6), PTH(1−7), PTH(1−8), and PTH(1−9)] joined to the PTH(15−31) domain via glycine linkers of lengths that preserved the overall chain length of 31 amino acids, and we tested these for cAMP signaling capacity. We found (data not shown) that only the PG5 analogue described here and containing PTH(1−9) connected by a pentaglycine linker to the PTH(15−31) domain was active. We also examined peptides with various lengths of glycine linker (two to eight glycines) between the PTH(1−9) and PTH(15−31) domains and found that the pentaglycine linker, as in PG5, resulted in optimal signaling activity; however, both shorter and

Table 2: Binding and cAMP Responses in HKRK-B28 Cells

	cAMP[b]			binding[c]	
peptide[a]	EC_{50} (nM)	E_{max}(obsd) (pmol/well)	*n*	IC_{50} (μM)	*n*
PTH(1−34)	0.97 ± 0.12	190 ± 8	3	0.0027 ± 0.0003	4
PTH(1−9)Gly5PTH(15−31)	2300 ± 400	139 ± 12	4	100 ± 34	5
PTH(1−9)Gly5[Arg[19]]PTH(15−31)	180 ± 40	179 ± 14	4	11 ± 1	5

[a] Peptides are described in Table 1. [b] EC_{50} and IC_{50} values were calculated using nonlinear regression analysis. The observed maximum cAMP responses [E_{max}(obsd)] were recorded at peptide concentrations of 10000 nM; the basal cAMP levels were 3.2 ± 0.2 pmol/well. [c] Competition binding studies utilized ^{125}I-bPTH(3−34) as a tracer radioligand. Values are the means (±sem) of the number of experiments indicated (*n*), each performed in duplicate.

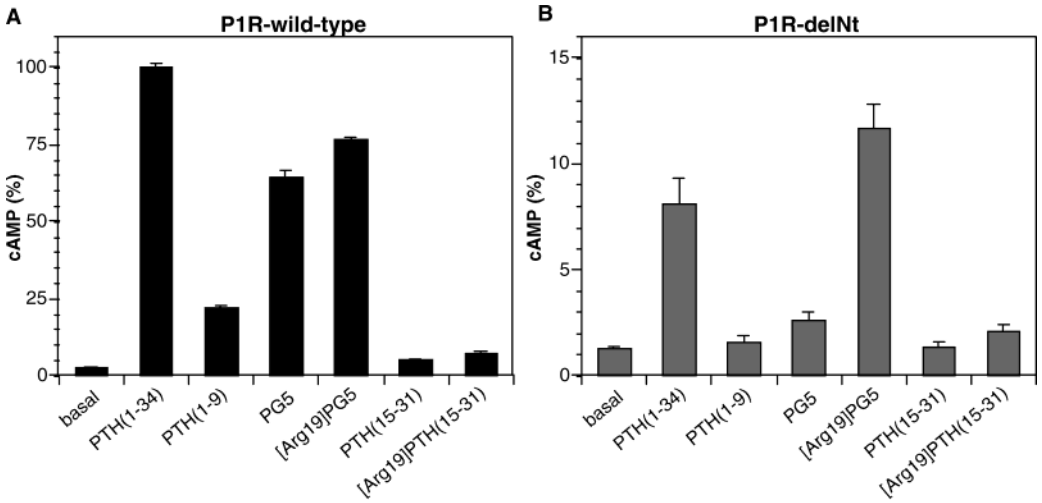

FIGURE 2: cAMP-stimulating properties of Gly-linked PTH analogues in COS-7 cells. The PTH analogues PG5 and [Arg[19]]PG5 (each at a concentration of 30 μM), along with the control peptides, PTH(1−34) (1 μM), PTH(1−14) (100 μM), PTH(1−9) (100 μM), PTH(15−31) (100 μM), and [Arg[19]]PTH(15−31) (100 μM), were evaluated in COS-7 cells transiently transfected with either the wild-type human PTH1 (A) or PTH1-delNt (B) for the capacity to stimulate cAMP formation. In each experiment, responses were calculated as a percentage of the response observed in that experiment for PTH(1−34) (1 μM) acting on the wild-type PTH1, the average of which was 192 ± 20 pmol/well ($n = 3$). Note that the ordinate scaling differs in panels A and B. The basal levels of cAMP (not subtracted) in cells expressing PTH1 and PTH1-delNt were 5.0 ± 0.7 and 2.6 ± 0.1 pmol/well, respectively. The differences between the responses observed for PG5 and [Arg[19]]PG5 on both PTH1 and PTH1-delNt were significant ($P = 0.001$ and 0.0001, respectively). Data (mean ± sem) were combined from three separate experiments, each performed in duplicate.

longer length linkers were tolerated and yielded potencies (EC_{50}s = 1−100 μM) similar to that of PG5, with only the diglycine linker failing to restore activity (the rank order of potency was 5Gly > 4Gly > 3Gly > 6Gly = 7Gly > 8Gly). These findings are generally consistent with the starting hypothesis stated above and confirm that the PTH(1−9) domain constitutes a minimum-length activation domain (*39*). They also suggest that the relative positioning of the N-terminal (1−9) signaling domain and the C-terminal (15−31) binding domain of the receptor-occupied PTH ligand is not fixed but somewhat flexible.

In COS-7 cells expressing wild-type PTH1, the response achieved by [Arg[19]]PG5 was slightly greater than that achieved by the same concentration (30 μM) of PG5 [77% and 64%, respectively, of the maximum response attained by PTH(1−34); Figure 2A]. This result is consistent with those obtained for these peptides in HKRK-B28 cells (Figure 1). In COS-7 cells expressing PTH1-delNt (Figure 2B), [Arg[19]]PG5 stimulated a 4-fold greater accumulation of cAMP than did the same concentration (30 μM) of PG5 ($P = 0.0001$), for which only a small (~2-fold, $P = 0.007$) increase in cAMP was observed. The control fragment peptides, PTH(1−9), PTH(15−31), and [Arg[19]]PTH(15−31), elicited little or no increase in cAMP accumulation (<2-fold, relative to basal) in cells expressing either PTH1 or PTH1-delNt. The Glu[19] → Arg substitution therefore enhances the affinity and potency of these Gly-linked peptides, and the effects are mediated via the J domain of the PTH1.

Circular Dichroism Spectroscopy. We used CD spectroscopy to assess the effect of the Glu[19] → Arg substitution on overall secondary structures of PG5 and [Arg[19]]PG5. The two analogues, along with the control peptides, PTH(1−34) and PTH(15−31), each consisting of a Glu[19] versus Arg[19] pairing, were analyzed in a solution of 50 mM phosphate containing 20% TFE. As indicated by the greater positive deflection at ~190 nm and the greater negative absorption at ~208 and 222 nm in the CD spectra of Figure 3, [Arg[19]]-PG5 was more helical than the Glu[19]-containing analogue, PG5. On the basis of the elipticity measured at 222 nm, the overall helical content of [Arg[19]]PG5 was calculated to be 5% greater than that of PG5 (Table 3). As expected, the Glu[19] → Arg substitution also increased the helicity of the control PTH(1−34), whereas, in contrast, it *decreased* the helicity of PTH(15−31) (Figure 3 and Table 3).

NMR Spectroscopy. All proton resonances of the PG5 and [Arg[19]]PG5 in the presence of DPC micelles were assigned using standard procedures. The fingerprint regions of TOCSY and NOESY spectra for two studied PTH analogues are shown in Figure 4. A large number of medium-range NOEs are depicted on NOESY spectra (Figure 4B,D). The differ-

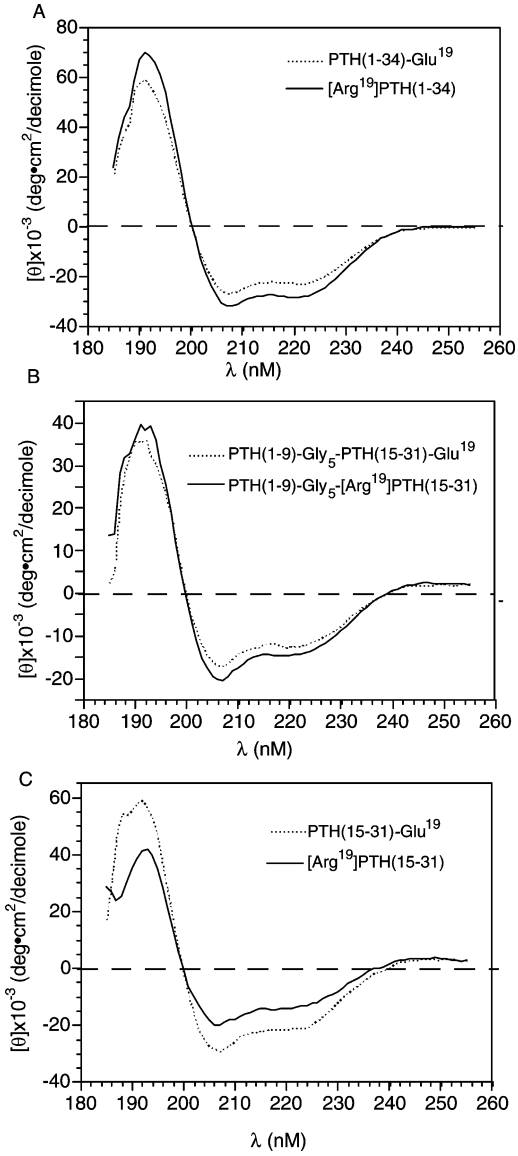

FIGURE 3: Circular dichroism spectroscopy. Spectra for the indicated PTH analogues, each at a peptide concentration of 50 μM, were recorded in 50 mM phosphate buffer, pH = 7.4, containing the helix-promoting organic solvent 2,2,2-trifluoroethanol (20% v/v), as described in Experimental Procedures and listed in Table 3.

ence between the observed chemical shift values of the α-protons (Hα) and the reported random coil Hα values provides a tentative estimate of a secondary structure. The secondary shifts were calculated for both peptides and are shown in Figure 5. The observed upfield shifts of Hα resonances indicate some helical content throughout the entire sequence of PG5 and [Arg^{19}]PG5. Namely, secondary shift values reaching almost −0.6 ppm in the C-terminal part of both analogues describe well-defined helices; negative secondary shifts of N-termini (residues Val^{2}−His^{9}), however, are more consistent with poorly ordered helical conformations. The five-glycine linker (residues Gly^{10}−Gly^{14}) between the C- and N-termini appears unstructured in both PTH analogues. Moreover, in agreement with CD results, the extent of the negative deviations for the region Leu^{15}−Met^{18} is larger for the Arg^{19}-substituted analogue than for PG5.

The observed NOESY connectivities are in complete agreement with the secondary shift pattern. The summary

Table 3: CD Effect of Arginine-19 on the Helical Structure in PTH Analogues

peptide[a]	$[\theta]_{222}$(obsd)[b] ($\times 10^{-3}$)	helical residues[c] (%)
PTH(1−34)	−22.8	52
[Arg^{19}]PTH(1−34)	−28.2	64
PTH(1−9)Gly5PTH(15−31)	−13.5	28
PTH(1−9)Gly5[Arg^{19}]PTH(15−31)	−15.6	33
PTH(15−31)	−23.2	48
[Arg^{19}]PTH(15−31)	−15.9	31

[a] Peptides are as described in Table 1. [b] Circular dichroism spectra were recorded in 50 mM phosphate buffer, pH 7.4, containing 2,2,2-trifluoroethanol (20% v/v), as described in Experimental Procedures and shown in Figure 3. [c] The helical content of each peptide was estimated using the equation $[[\theta]_{222}(\text{obsd})/[\theta]_{222}(\text{max})] \times 100$, where $[\theta]_{222}$(obsd) is the mean residue elipticity at 222 nm observed for that peptide and $[\theta]_{222}$(max) is −44000, the mean residue elipticity at 222 nm reported for a model helical peptide (*19*).

of all NOESY resonances for PG5 and [Arg^{19}]PG5, relevant for determination of the peptide secondary structures, is given in Figure 6. Strong consecutive NOEs are observed between resolved peaks throughout the entire sequence, starting from residue Val^{2} in both peptides. The presence of all possible sequential NOEs suggests that the peptides are, overall, well structured. A large number of αH(i)−NH(i + 3), αH(i)−βH(i + 3), and αH(i)−NH(i + 4) resonances define structured, α-helical segments in the C-termini of the peptides, starting from residue Gly^{14}. A slightly higher number of helical NOEs are observed for the Arg^{19}-substituted analogue, relative to the Glu^{19} analogue. For both peptides, the N-terminus displays fewer α-helical NOEs than observed in the C-terminus, and resonance peaks corresponding to the five glycine linker residues could not be resolved. A total of 275 and 285 informative NOE-derived distance constraints were used in distance geometry calculations for PG5 and [Arg^{19}]PG5, respectively.

The metric matrix DG calculations were repeated 120 times for each peptide, producing approximately 70 structures for each analogue that fulfilled the experimental NMR data. No violations exceeded 0.3 Å for individual conformations. The secondary shift data, indicating the presence of helices, were not used as restraints during DG calculations. Moreover, metric matrix DG calculations do not take into account partial charges of the amide and carbonyl groups. Forty calculated DG structures, superimposed in Glu^{22}−Leu^{28} region (RMSD < 1 Å), are shown in Figure 7. Visual examination of the conformational space sampled by DG calculations shows a strong α-helical segment in the C-terminal part of the studied peptides, extending approximately from residue Asn^{16} to Val^{31}. Analyzing the ϕ and ψ dihedral angle order parameter distribution of the resulting DG structures (Figure 8) illustrates that PG5 has relatively low order parameter values for residues Met^{18} and Glu^{19}, indicating some disorder at these positions. Such a hinge is not observed for the Arg^{19}-substituted analogue. This result is consistent with CD and secondary shift observations and suggests a slightly increased helical content for the [Arg^{19}]PG5 peptide between residues 15 and 20. The N-termini of both peptides are poorly defined, mostly extended, but a helical structure is still somewhat predominant between residues Glu^{4} and Met^{8} (Figure 7), where dihedral angle order parameters are high for both analogues (Figure 8). The DG calculations confirm the

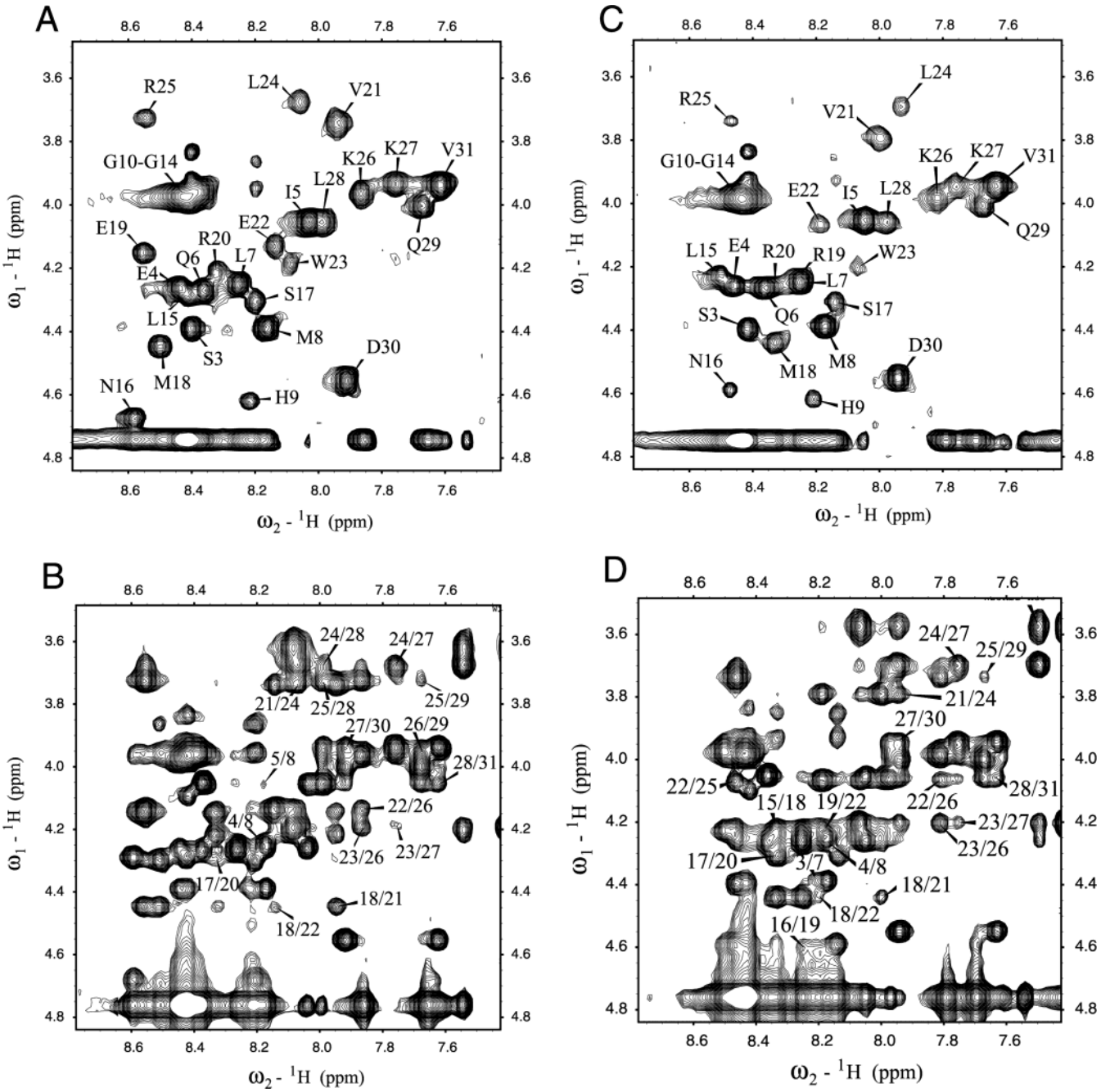

FIGURE 4: NMR spectroscopy. Expended portions of the fingerprint regions of the TOCSY (A, C) and NOESY (B, D) spectra of PTH(1−9)Gly5PTH(15−31) (A, B) and PTH(1−9)Gly5[Arg^{19}]PTH(15−31) (C, D) analogues in aqueous solutions (pH = 6.5) in the presence of DPC micelles are shown. The assignments are depicted for TOCSY resonances in the amide region; some helical, αH(i)−NH(i + 2), αH(i)−NH(i + 3), and αH(i)−NH(i + 4), connectivities are indicated for NOESY cross-peaks.

unstructured, extended backbone conformation for Gly^{10}−Gly^{14} regions of studied PTH analogues.

One representative DG structure for each peptide was further refined using MD simulation. During the simulation no significant change was observed in the secondary structure of the peptides, as shown in Figure 9. The dihedral angles of the C-terminus (Leu^{15}−Val^{31}) of both peptides converged toward standard α-helical values and were maintained throughout the simulation; no hinge point was observed for PTH(1−9)Gly5PTH(15−31) around residues Met^{18} and Glu^{19}. In addition, the poorly defined structures of the N-terminal regions, obtained from DG, adopted a well-defined helical turn encompassing residues Ser^{3}−Met^{8} in both PTH analogues. The five glycine (Gly^{10}−Gly^{14}) linkers maintained extended conformations, as shown in Figure 9. After 700 ps of MD, the amphipathic helices of the analogues oriented themselves similarly at the water−decane interface: the helical hydrophobic face was directed toward the decane layer (Leu^{7}, Met^{8}, Val^{21}, Leu^{24}, Leu^{28}, Val^{31}), and the side chains of the charged and hydrophilic residues (Glu^{4}, Glu^{19}/Arg^{19}, Glu^{22}, Lys^{26}, Asp^{30}) projected toward the water (Figure 9).

Molecular Models of the Ligand/Receptor Complexes. The total energies for the receptor−ligand complex, incorporating PG5 and [Arg^{19}]PG5, were calculated using the GROMACS 3.1.3 program. A similar drop in total energy was detected during the first 40 ps for both systems. The equilibrated energies, observed for the last 500 ps of MD simulations,

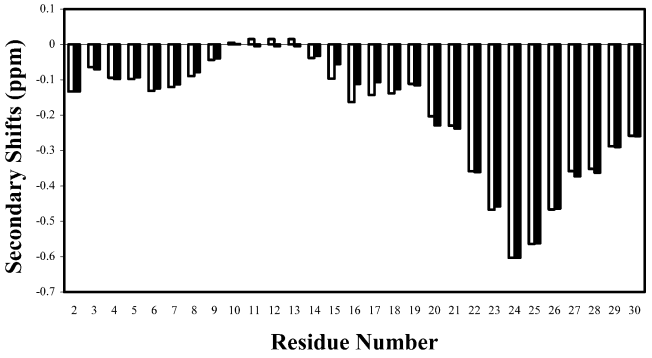

FIGURE 5: Secondary shifts. Secondary shift (Hα) values are shown for the PTH(1−9)Gly5PTH(15−31) analogue (black bars) and PTH(1−9)Gly5[Arg^{19}]PTH(15−31) peptide (white bars) in aqueous solution (pH = 6.5) in the presence of DPC micelles (180 mM). The chemical shifts were measured at 35 °C and referenced to TSP.

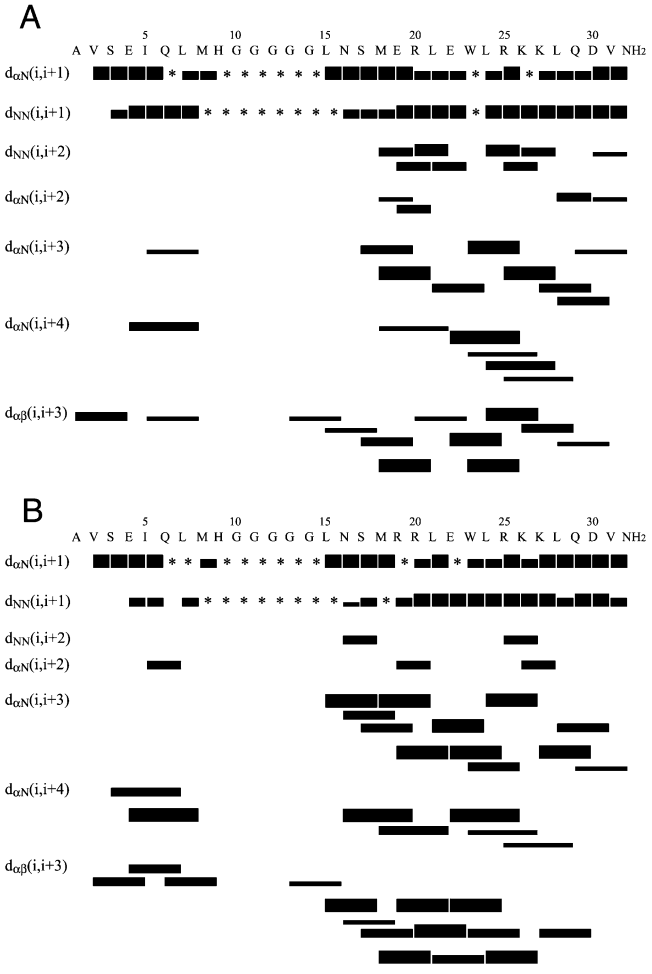

FIGURE 6: NOESY connectivities. A summary of NOESY connectivities is shown for (A) PTH(1−9)Gly5PTH(15−31) and (B) PTH(1−9)Gly5[Arg^{19}]PTH(15−31) analogues. Peaks are grouped in three classes (strong, medium, and weak) on the basis of their integrated volumes. An asterisk indicates a cross-peak, which could not be identified due to resonance overlap.

were also comparable for both receptor−ligand complexes. The topological orientations of the PG5 and [Arg^{19}]PG5 ligands and the major binding interactions with PTH1 are shown in Figure 10.

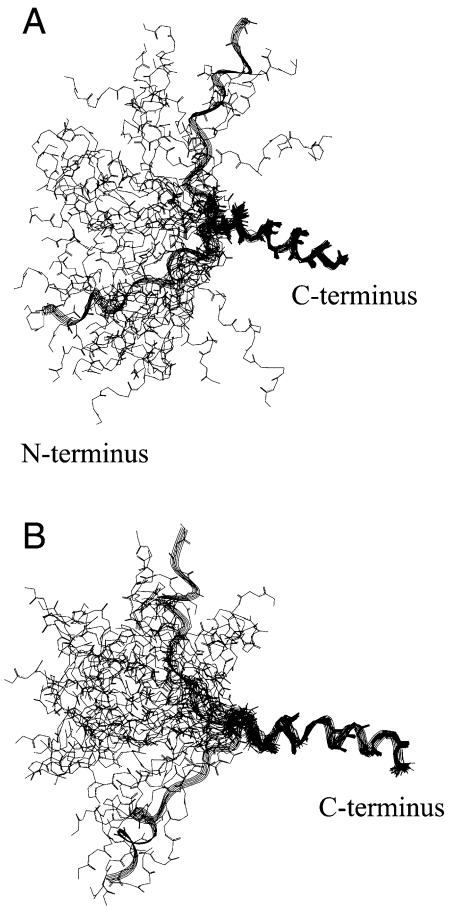

FIGURE 7: Distance geometry calculations. A superposition of 40 structures, obtained from DG calculations, for (A) PTH(1−9)-Gly5PTH(15−31) (RMSD = 0.9 Å for the Glu^{22}−Leu^{28} region) and (B) PTH(1−9)Gly5[Arg^{19}]PTH(15−31) analogues (RMSD = 0.8 Å for the Glu^{22}−Leu^{28} region) is shown. Two random structures for each peptide are depicted with ribbons; the C-terminus of both PTH analogues exhibits α-helical conformation, while N-termini display almost extended, poorly defined helical segments.

DISCUSSION

One of the main hypotheses investigated in this study is that the C-terminal binding domain of PTH(1−31) functions primarily to anchor the otherwise weakly binding N-terminal signaling domain of PTH to the receptor, such that the key N-terminal residues of PTH can effectively engage the extracellular loop/transmembrane domain (J) region of the receptor to induce activation. As a test of this hypothesis, we used a tethered ligand approach, in which we started with the inactive PTH(15−31) binding domain and asked whether activity could be recovered by connecting to it, via a flexible glycine linker, a minimum length N-terminal activation domain, which by itself is inactive due to weak binding affinity. Additionally, we addressed the role of residue 19 of the ligand in the receptor interaction process, as our previous studies have indicated an important but complex role for this residue in the receptor interaction process, involving possible direct contacts with the receptor (*14*), secondary structure of the ligand (*15*), and intramolecular interactions with the N-terminal signaling domain of the ligand (*40*). We thus prepared a PG5 analogue containing Arg (versus Glu) at position 19 to explore possible affinity-enhancing effects of this substitution in a ligand containing a flexible midregion linker. The Arg^{19} modification, relative

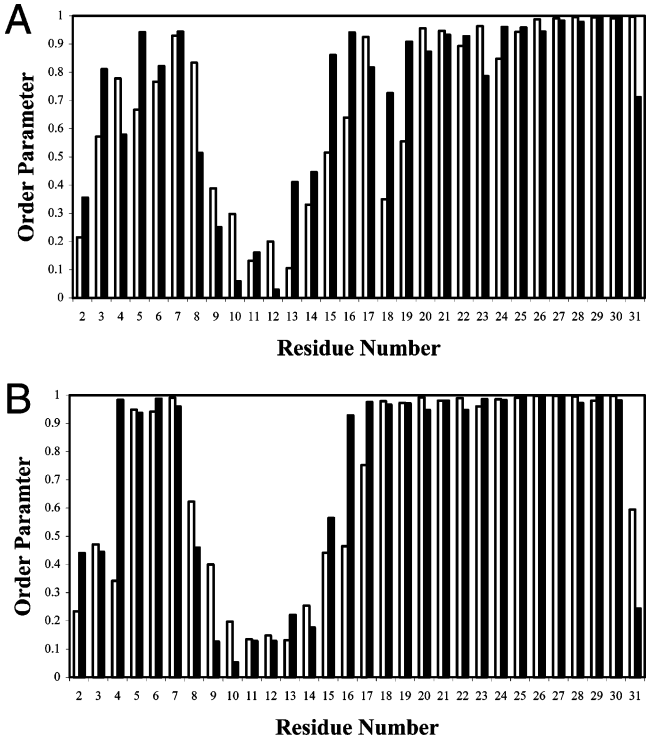

FIGURE 8: Order parameter values. Order parameter values for ϕ (white bars) and ψ (black bars) backbone dihedral angles calculated for the ensembles of structures, obtained from the DG calculations, for (A) the PTH(1−9)Gly5PTH(15−31) analogue and (B) the PTH-(1−9)Gly5[Arg^{19}]PTH(15−31) peptide. For the Arg^{19}-substituted analogue order parameters remain close to 1 throughout residues 16 and 30.

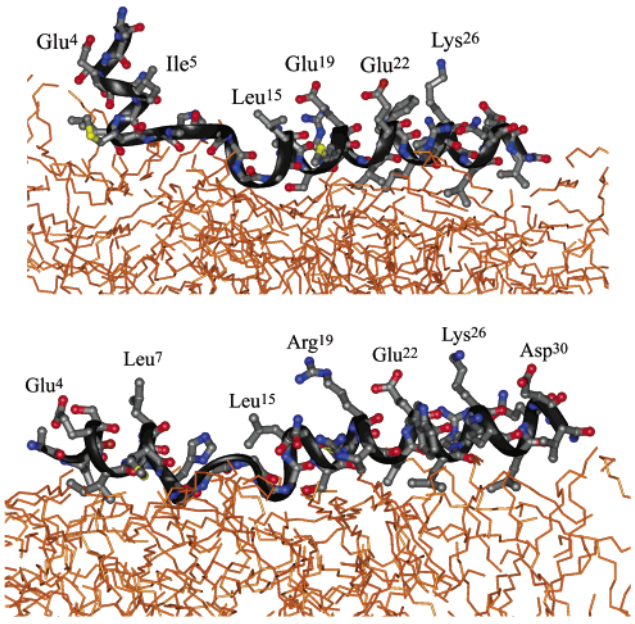

FIGURE 9: Peptide conformations at the water/decane interface. The final conformations of the two PTH analogues studied, PTH(1−9)Gly5PTH(15−31) (top) and PTH(1−9)Gly5[Arg^{19}]PTH(15−31) (bottom), obtained from an NOE-restrained MD simulation (700 ps) in a water/decane membrane mimetic solvent box with periodic boundary conditions are displayed. The water phase is not shown for simplicity. The decane phase is depicted in golden brown sticks. The receptor fragments are shown with dark gray ribbons with the N-terminus oriented to the left; atoms for the receptor amino acids are color coded (red = oxygen, blue = nitrogen, yellow = sulfur, and light gray = carbon), and some side chains are labeled in three-letter code.

to Glu^{19}, enhanced PG5 binding affinity by 9-fold and similarly enhanced cAMP potency in COS-7 cells expressing both the intact PTH1 and PTH1-delNt, which lacks most of the amino-terminal extracellular domain. These findings confirm the hypothesis that the affinity-enhancing effect of the Glu^{19} → Arg substitution is mediated via the J domain of the PTH1 and also indicate that the effect requires a residue, or residues, in the PTH(1−9) region, as the substitution has no effect on the binding affinity of PTH-(15−34) (*14*). One possible explanation for these results is that the interaction of the (1−9) portion of the ligand with the receptor results in the positioning of the Arg^{19} side chain within a favorable location in the receptor; such positioning would not occur in the context of the PTH(15−31) analogue.

Structural Consequences of Arg^{19} and the Pentaglycine Linker. We also examined the possibility that the Arg^{19} modification induces structural changes in PG5 and thereby indirectly contributes to function, as we noted previously in our studies of this modification in [M]PTH(1−20) [[Ala^{1,3,12},-Gln^{10},Har^{11},Trp^{14},X^{19}]PTH(1−20)amide] analogues. Our current circular dichroism analyses revealed that, relative to Glu^{19}, Arg^{19} slightly increased helicity in PG5, whereas it decreased helicity in the truncated PTH(15−31) fragment (Table 1). The Glu^{19} → Arg substitution, therefore, has a helix-*stabilizing* effect when residues (1−14) are present, even if residues 10−14 are glycines (Figure 3A,B), whereas it has a helix-*destabilizing* effect when residues 1−14 are absent, as in PTH(15−31) (Figure 3C).

To determine the precise location of secondary structural changes in PG5 and [Arg^{19}]PG5, we used high-resolution NMR spectroscopy, performed with the peptides dissolved in DPC micelles, a solvent system that mimics the membrane environment of the native receptor (*41*−*45*). As revealed by the similar secondary shift patterns (Figure 5), both PG5 and [Arg^{19}]PG5 adopt similar secondary structures, characterized by a well-defined C-terminal helix starting right after the pentaglycine linker and a mostly extended N-terminal conformation with some nascent helix in residues 1−9. Not surprisingly, the pentaglycine chain was completely unstructured in both analogues. The only structural difference observed for the two peptides was that [Arg^{19}]PG5 was slightly more helical in the residue 15−20 region than was PG5 (Figure 5). This observation is consistent with the notion that the helix-stabilizing effect of Arg^{19} propagates N-terminally (*15*). The NOESY connectivities and DG calculations support these conclusions: for the Arg^{19}-substituted analogue, a greater number of helical NOEs were detected (Figure 6), and the order parameter values were higher (Figure 8) between residues 15 and 20. Considered together with our in vitro functional data, these NMR data indicate a clear positive correlation between helicity in the residue 15−20 region of the ligand and biological activity and, thus, support the hypothesis that the helix is the preferred biological conformation for this region of parathyroid hormone (*15*). Although the helix-stabilizing effect of the Glu^{19} → Arg substitution in [Arg^{19}]PG5 propagates N-terminally, it stops at the pentaglycine linker and has no prominent effect on the secondary structure of residues 1−9.

MD Simulations of the Receptor−*Ligand Complexes.* We used molecular dynamics simulation to analyze potential differences in the binding modes used by PG5 and [Arg^{19}]-PG5, specifically focusing on the component of the interac-

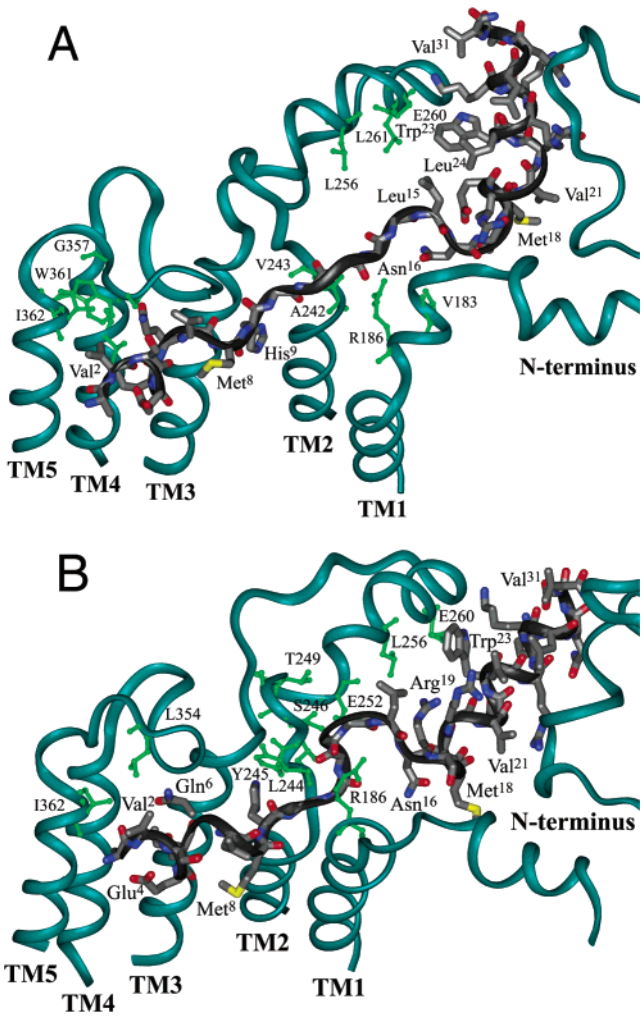

FIGURE 10: MD simulations of the receptor−ligand complexes. An illustration of some of the interactions between the PTH analogues studied, (A) PTH(1−9)Gly5PTH(15−31) and (B) PTH(1−9)Gly5[Arg^{19}]PTH(15−31), and the PTH1 receptor is given. For each complex the receptor cross section is taken for better view; only TM2-EC1-TM3, TM4-EC2-TM5, TM1, and part of the N-terminus of PTH1 are displayed in a dark greenish blue ribbon. Some receptor side chains, interacting with the ligands, are shown in light green sticks and denoted in one-letter code. The backbones of the ligands are shown in gray sticks and are color-coded (red = oxygen, blue = nitrogen, and light gray = carbon). Side chains are displayed for both (A) PTH(1−9)Gly5PTH(15−31) and (B) PTH(1−9)Gly5[Arg^{19}]PTH(15−31) peptides. The residues of the ligands are shown in three-letter code.

tion involving the PTH1 J domain, the structure of which can be approximated from the rhodopsin template (little or no structural information is available for the PTH1 N domain). As initial constraints, we used the established cross-linking points of Val^2/Met425(TM6) (*37*) and Lys^{13}/Arg186 (TM1/D domain boundary) (*38*). Subsequent analysis of the MD simulations revealed the binding modes used by the N-terminal helices of the two analogues to be similar: the helix lies along the extracellular face of the seven transmembrane domain bundle and is partly covered by portions of extracellular loops (ECs) 2 and 3. Val^2 of the ligand, a key receptor activation residue (*46*), contacts hydrophobic side chains from extracellular loop (ECL) 2 (Trp361, Ile362, Leu354, Ser355, Gly357) and ECL3 (Gln440, Leu436, Met441, H442), consistent with our previous PTH(1−34)/PTH1 models (*36*, *47*) (Figure 10). Although both PG5 and [Arg^{19}]PG5 maintain their overall bihelical conformation throughout the 500 ps of MD simulation, some changes are observed in the C-terminal helices. Specifically, the PG5 α-helix extends N-terminally only to Glu^{19} (Figure 10A), whereas the helix of the Arg^{19}-substituted analogue extends N-terminally to Asn^{16} (Figure 10B). This result is in accord with our biological and NMR data, which suggest that increased helicity in the residue 15−20 region of the Arg^{19}-containing PG5 analogue correlates with its stronger affinity and potency.

In the model, the Arg^{19} side chain projects away from the seven TM bundle and toward the EC1 loop to form Coulombic interactions with EC1 residues Glu260 and Glu252 (Figure 10B). These energetically favorable charge−charge contacts may account for at least some of the increased binding affinity of the Arg^{19}-containing ligand, as no such contacts could be identified for Glu^{19} of PG5. No specific intramolecular side chain−side chain interactions could be identified within the receptor-bound ligand that would explain the enhanced helicity of the residue 15−20 region of the Arg^{19}-substituted peptide. The structural difference between the binding domains of the two ligands may be due to a helix-destabilizing effect caused by Glu^{19}. Indeed, our simulation data show that the side chain of Glu^{19} folds back toward the ligand backbone and interacts with Arg^{20}; this interaction could partially account for the distorted helical turn at position 19, as well as the almost extended secondary structure of Leu^{15}−Glu^{19}, in the PG5 analogue (Figure 10A). The only specific contact sites for residue 19 of the PG5 peptides are found within the EC1 loop, as noted above. This finding differs somewhat from the cross-linking data, which showed that the benzoylphenylalanine (Bpa) moieties of [Bpa^{19}]PTHrP(1−36) and [Bpa^{19}]PTH(1−21) analogues contact the segment (His^{225}−Lys^{240}) at the extracellular end of TM2: no such interaction was observed in the PG5−PTH1 and [Arg^{19}]PG5−PTH1 complexes. This apparent discrepancy could be due to the relatively large cross-linking radius (∼10 Å) for the Bpa moiety, to differences in the chemical natures of the position 19 side chains (hydrophilic Glu/Arg vs hydrophobic Bpa), and/or to variations in the backbone conformations of the ligands [e.g., the unstructured pentaglycine 10−14 segments vs more rigid structures for the PTHrP(1−36) and PTH(1−20) analogues]. Further experimental constraints would be necessary in order to more fully elucidate and account for differences in the binding mechanisms used by these and other ligand analogues that bind to the PTH1.

ACKNOWLEDGMENT

We thank Ashok Khatri for peptide synthesis and Henry M. Kronenberg and John T. Potts for insightful comments.

REFERENCES

1. Nussbaum, S. R., Rosenblatt, M., and Potts, J. T., Jr. (1980) Parathyroid hormone renal receptor interactions. Demonstration of two receptor-binding domains, *J. Biol. Chem. 255*, 10183−10187.
2. Abou-Samra, A. B., Uneno, S., Jueppner, H., Keutmann, H., Potts, J. T., Jr., Segre, G. V., and Nussbaum, S. R. (1989) Non-homologous sequences of parathyroid hormone and the parathyroid hormone related peptide bind to a common receptor on ROS 17/2.8 cells, *Endocrinology 125*, 2215−2217.

3. Caulfield, M. P., McKee, R. L., Goldman, M. E., Duong, L. T., Fisher, J. E., Gay, C. T., DeHaven, P. A., Levy, J. J., Roubini, E., Nutt, R. F., et al. (1990) The bovine renal parathyroid hormone (PTH) receptor has equal affinity for two different amino acid sequences: the receptor binding domains of PTH and PTH-related protein are located within the 14−34 region, *Endocrinology 127*, 83−87.
4. Nutt, R. F., Caulfield, M. P., Levy, J. J., Gibbons, S. W., Rosenblatt, M., and McKee, R. L. (1990) Removal of partial agonism from parathyroid hormone (PTH)-related protein-(7−34)NH2 by substitution of PTH amino acids at positions 10 and 11, *Endocrinology 127*, 491−493.
5. Luck, M. D., Carter, P. H., and Gardella, T. J. (1999) The (1−14) fragment of parathyroid hormone (PTH) activates intact and amino-terminally truncated PTH-1 receptors, *Mol. Endocrinol. 13*, 670−680.
6. Shimizu, M., Potts, J. T., and Gardella, T. J. (2000) Minimization of parathyroid hormone. Novel amino-terminal parathyroid hormone fragments with enhanced potency in activating the type-1 parathyroid hormone receptor, *J. Biol. Chem. 275*, 21836−21843.
7. Whitfield, J. F., Morley, P., Willick, G. E., Ross, V., MacLean, S., Barbier, J. R., Isaacs, R. J., and Ohannessian-Barry, L. (1997) Comparison of the ability of recombinant human parathyroid hormone, rhPTH-(1−84), and hPTH-(1−31)NH2 to stimulate femoral trabecular bone growth in ovariectomized rats, *Calcif. Tissue Int. 60*, 26−29.
8. Neer, R. M., Arnaud, C. D., Zanchetta, J. R., Prince, R., Gaich, G. A., Reginster, J. Y., Hodsman, A. B., Eriksen, E. F., Ish-Shalom, S., Genant, H. K., Wang, O., and Mitlak, B. H. (2001) Effect of parathyroid hormone (1−34) on fractures and bone mineral density in postmenopausal women with osteoporosis, *N. Engl. J. Med. 344*, 1434−1441.
9. Marx, U. C., Adermann, K., Bayer, P., Forssmann, W. G., and Rösch, P. (2000) Solution structures of human parathyroid hormone fragments hPTH(1−34) and hPTH(1−39) and bovine parathyroid hormone fragment bPTH(1−37), *Biochem. Biophys. Res. Commun. 267*, 213−220.
10. Pellegrini, M., Royo, M., Rosenblatt, M., Chorev, M., and Mierke, D. F. (1998) Addressing the tertiary structure of human parathyroid hormone-(1−34), *J. Biol. Chem. 273*, 10420−10427.
11. Hoare, S. R., Gardella, T. J., and Usdin, T. B. (2001) Evaluating the signal transduction mechanism of the parathyroid hormone 1 receptor. Effect of receptor-G-protein interaction on the ligand binding mechanism and receptor conformation, *J. Biol. Chem. 276*, 7741−7753.
12. Condon, S. M., Morize, I., Darnbrough, S., Burns, C. J., Miller, B. E., Uhl, J., Burke, K., Jariwala, N., Locke, K., Krolikowski, P. H., Kumar, N. V., and Labaudiniere, R. F. (2000) The Bioactive Conformation of Human Parathyroid Hormone. Structural Evidence for the Extended Helix Postulate, *J. Am. Chem. Soc. 122*, 3007−3014.
13. Jin, L., Briggs, S. L., Chandrasekhar, S., Chirgadze, N. Y., Clawson, D. K., Schevitz, R. W., Smiley, D. L., Tashjian, A. H., and Zhang, F. (2000) Crystal structure of human parathyroid hormone 1−34 at 0.9-A resolution, *J. Biol. Chem. 275*, 27238−27244.
14. Shimizu, M., Shimizu, N., Tsang, J. C., Petroni, B. D., Khatri, A., Potts, J. T., Jr., and Gardella, T. J. (2002) Residue 19 of the Parathyroid Hormone (PTH) Modulates Ligand Interaction with the Juxtamembrane Region of the PTH-1 Receptor, *Biochemistry 41*, 13224−13233.
15. Piserchio, A., Shimizu, N., Gardella, T. J., and Mierke, D. F. (2002) Residue 19 of the parathyroid hormone: structural consequences, *Biochemistry 41*, 13217−13223.
16. Bergwitz, C., Jusseaume, S. A., Luck, M. D., Juppner, H., and Gardella, T. J. (1997) Residues in the membrane-spanning and extracellular loop regions of the parathyroid hormone (PTH)-2 receptor determine signaling selectivity for PTH and PTH-related peptide, *J. Biol. Chem. 272*, 28861−28868.
17. Takasu, H., Gardella, T. J., Luck, M. D., Potts, J. T., and Bringhurst, F. R. (1999) Amino-terminal modifications of human parathyroid hormone (PTH) selectively alter phospholipase C signaling via the type 1 PTH receptor: implications for design of signal-specific PTH ligands, *Biochemistry 38*, 13453−13460.
18. Carter, P. H., Juppner, H., and Gardella, T. J. (1999) Studies of the N-terminal region of a parathyroid hormone-related peptide (1−36) analog: receptor subtype-selective agonists, antagonists, and photochemical cross-linking agents, *Endocrinology 140*, 4972−4981.
19. Yang, J. T., Wu, C. S., and Martinez, H. M. (1986) Calculation of protein conformation from circular dichroism, *Methods Enzymol. 130*, 208−269.
20. Fasman, G. D. (1996) *Circular Dichroism and the Conformational Analysis of Biomolecules*, Plenum, New York.
21. Braunschweiler, L., and Ernst, R. R. (1983) Coherence Transfer by Isotropic Mixing: Application to Proton Correlation Spectroscopy, *J. Magn. Reson. 53*, 521−528.
22. Bax, A., and Davis, D. G. (1985) MLEV-17 Based Two-Dimensional Homonuclear Magnetization Transfer Spectroscopy, *J. Magn. Reson. 65*, 355−360.
23. Macura, S., Huang, Y., Suter, D., and Ernst, R. R. (1981) Two-Dimensional Chemical Exchange and Cross-Relaxation Spectroscopy of Coupled Nuclear Spins, *J. Magn. Reson. 43*, 259−281.
24. Jeener, J., Meier, B. H., Bachmann, P., and Ernst, R. R. (1979) Investigation of Exchange Processes by Two-Dimensional NMR Spectroscopy, *J. Chem. Phys. 71*, 4546−4553.
25. Piotto, M., Saudek, V., and Sklenar, V. (1992) Gradient-tailored excitation for single-quantum NMR spectroscopy of aqueous solutions, *J. Biomol. NMR 2*, 661−665.
26. Bodenhausen, G., Vold, R. L., and Vold, R. R. (1980) *J. Magn. Reson. 37*, 93−106.
27. Delaglio, F., Grzesiek, S., Vuister, G. W., Zhu, G., Pfeifer, J., and Bax, A. (1995) NMRPipe: a multidimensional spectral processing system based on UNIX pipes, *J. Biomol. NMR 6*, 277−293.
28. Goddard, T. D., and Kneller, D. G. (2001) Sparky 3.0, University of California, San Francisco.
29. Wishart, D. S., Sykes, B. D., and Richards, F. M. (1992) The chemical shift index: a fast and simple method for the assignment of protein secondary structure through NMR spectroscopy, *Biochemistry 31*, 1647−1651.
30. Wüthrich, K., Billeter, M., and Braun, W. (1983) Pseudo-structures for the 20 common amino acids for use in studies of protein conformations by measurements of intramolecular proton−proton distance constraints with nuclear magnetic resonance, *J. Mol. Biol. 169*, 949−961.
31. Havel, T. F. (1991) An evaluation of computational strategies for use in the determination of protein structure from distance geometry constraints obtained by nuclear magnetic resonance, *Prog. Biophys. Mol. Biol. 56*, 43−78.
32. Mierke, D. F., Scheek, R. M., and Kessler, H. (1994) Coupling Constant Restraints in Ensemble Calculations, *Biopolymers 34*, 559−563.
33. Mierke, D. F., Geyer, A., and Kessler, H. (1994) Coupling constants and hydrogen bonds as experimental restraints in a distance geometry refinement protocol, *Int. J. Pept. Protein Res. 44*, 325−331.
34. Havel, T. F. (1990) The sampling properties of some distance geometry algorithms applied to unconstrained polypeptide chains: a study of 1830 independently computed conformations, *Biopolymers 29*, 1565−1585.
35. Berendsen, H. J. C., van der Spoel, D., and van Buuren, R. (1995) GROMACS: A Message Passing Parallel Molecular Dynamics Implementation, *Comput. Phys. Commun. 95*, 43−56.
36. Rölz, C., Pellegrini, M., and Mierke, D. F. (1999) Molecular Characterization of the Receptor−Ligand Complex for Parathyroid Hormone, *Biochemistry 38*, 6397−6405.
37. Behar, V., Bisello, A., Rosenblatt, M., and Chorev, M. (1999) Direct identification of two contact sites for parathyroid hormone (PTH) in the novel PTH-2 receptor using photoaffinity cross-linking, *Endocrinology 140*, 4251−4261.
38. Adams, A. E., Bisello, A., Chorev, M., Rosenblatt, M., and Suva, L. J. (1998) Arginine 186 in the extracellular N-terminal region of the human parathyroid hormone 1 receptor is essential for contact with position 13 of the hormone, *Mol. Endocrinol. 12*, 1673−1683.
39. Shimizu, M., Carter, P. H., and Gardella, T. J. (2000) Autoactivation of type-1 parathyroid hormone receptors containing a tethered ligand, *J. Biol. Chem. 275*, 19456−19460.
40. Gardella, T. J., Luck, M. D., Wilson, A. K., Keutmann, H. T., Nussbaum, S. R., Potts, J. T., Jr., and Kronenberg, H. M. (1995) Parathyroid hormone (PTH)-PTH-related peptide hybrid peptides reveal functional interactions between the 1−14 and 15−34 domains of the ligand, *J. Biol. Chem. 270*, 6584−6588.
41. Sargent, D. F., and Schwyzer, R. (1986) Membrane Lipid Phase as Catalyst for peptide-Receptor Interaction, *Proc. Natl. Acad. Sci. U.S.A. 83*, 5774−5778.

42. Schwyzer, R. (1991) Peptide-membrane interactions and a new principle in quantitative structure−activity relationships, *Biopolymers 31*, 785−792.
43. Schwyzer, R. (1992) How Do Peptides Interact with Lipid Membranes and How Does This Affect Their Biological Activity, *Braz. J. Med. Biol. Res. 25*, 1077−1089.
44. Moroder, L., Romano, R., Guba, W., Mierke, D. F., Kessler, H., Delporte, C., Winand, J., and Christophe, J. (1993) New evidence for a membrane-bound pathway in hormone receptor binding, *Biochemistry 32*, 13551−13559.
45. Inooka, H., Ohtaki, T., Kitahara, O., Ikegami, T., Endo, S., Kitada, C., Ogi, K., Onda, H., Fujino, M., and Shirakawa, M. (2001) Conformation of a peptide ligand bound to its G-protein coupled receptor, *Nat. Struct. Biol. 8*, 161−165.
46. Lee, C., Luck, M. D., Juppner, H., Potts, J. T., Jr., Kronenberg, H. M., and Gardella, T. J. (1995) Homolog-scanning mutagenesis of the parathyroid hormone (PTH) receptor reveals PTH-(1−34) binding determinants in the third extracellular loop, *Mol. Endocrinol. 9*, 1269−1278.
47. Monticelli, L., Mammi, S., and Mierke, D. F. (2002) Molecular characterization of a ligand-tethered parathyroid hormone receptor, *Biophys. Chem. 95*, 165−172.

BI036127T